A new family of deployable mechanisms based on the Hoekens linkage

Article *in* Mechanism and Machine Theory · January 2014

CITATIONS
2

READS
771

4 authors, including:

Shengnan Lu
Beihang University (BUAA)
13 PUBLICATIONS **12** CITATIONS
SEE PROFILE

Dimiter Zlatanov
Università degli Studi di Genova
55 PUBLICATIONS **1,080** CITATIONS
SEE PROFILE

Rezia M. Molfino
Università degli Studi di Genova
260 PUBLICATIONS **730** CITATIONS
SEE PROFILE

Mechanism and Machine Theory 73 (2014) 130–153

Contents lists available at ScienceDirect

Mechanism and Machine Theory

journal homepage: www.elsevier.com/locate/mechmt

A new family of deployable mechanisms based on the Hoekens linkage ☆

Shengnan Lu [a,b], Dimiter Zlatanov [a,*], Xilun Ding [b], Rezia Molfino [a]

[a] PMAR Robotics, University of Genoa, Genoa 16145, Italy
[b] Robotics Institute, Beihang University, Beijing 100191, China

ARTICLE INFO

Article history:
Received 24 July 2013
Received in revised form 5 October 2013
Accepted 17 October 2013
Available online xxxx

Keywords:
Deployable prism mechanisms
Straight-line linkage
Deployable unit
Magnification ratio

ABSTRACT

The paper proposes a family of novel deployable prism mechanisms based on the Hoekens straight-line linkage. The prism can be deployed and compacted in a single dimension. First, a novel planar deployable unit is described, and its kinematics, statics, and singularities are analyzed. The magnification ratio is calculated as a function of the physical size of the links. Then, we describe the possibility and the principles of combining multiple unit mechanisms into a larger deployable mechanism. This process allows the creation of a series of deployable mast units, which are used to design the novel family of deployable prism mechanisms, each with one degree of freedom and an invariable cross section. The best choice of actuator is determined through static analysis and the structural behavior of the mechanism is analyzed by simulation.

1. Introduction

Deployable mechanisms (DMs) based on linkages have been studied by a number of researchers over the past decades [1–5]. Several types have been proposed such as Wohlhart's polyhedral star-transformer [6], Hoberman's polyhedral mechanism [7], and the cubic/octahedral linkages which are described by Kipper [8]. Deployable mechanisms can have different types of expansion patterns, e.g., one-dimensional, planar, polyhedral, and cambered. Deployable/foldable prisms represent an important example of one-dimensional DMs. They are widely used in large space structures and can conceivably find applications as fixture mechanisms in manufacturing, as well as in civil engineering applications. The formation of deployable masts assembled from octahedral trusses has been addressed by Chen et al. [9]. Nagaraj et al. studied the kinematics and DOF of a deployable mast based on the scissor-like element [10]. Ding and Yang proposed a novel mast mechanism using spatial polyhedral linkages arranged along radial axes [11].

In space applications, there are high costs associated with increasing the size and mass of objects taken into orbit. These limitations determine a need to fully utilize the internal space of the deployed structure. In all previously proposed deployable masts based on linkages, however, the cross-sectional area changes during the deployment process. Once the mechanism is moved, the two dimensions are changed simultaneously. This is often a drawback: the internal space cannot be well utilized because it is variable and masts with constant cross-section are preferable. Similarly, in the auto industry it is expected for a flexible fixture to have the ability to reconfigure itself to fit the length of the workpiece, while remaining of constant width. Herein, we present a new family of deployable prism mechanism, in which one-DOF planar polygonal linkages are mounted on the faces and assembled using four revolute joints at the vertices. Unlike other prism DMs, the cross section of the mechanism remains constant during the deployment movement.

☆ A preliminary version of this research was presented at the 2nd IFToMM Symposium on Mechanism Design for Robotics, 12–14 October 2012, Beihang University, Beijing, China.

* Corresponding author.
E-mail addresses: lvshengnan5@gmail.com (S. Lu), zlatanov@dimec.unige.it (D. Zlatanov), xlding@buaa.edu.cn (X. Ding), molfino@dimec.unige.it (R. Molfino).

0094-114X/$ – see front matter © 2013 Elsevier Ltd. All rights reserved.
http://dx.doi.org/10.1016/j.mechmachtheory.2013.10.007

The paper is organized as follows. The kinematics and static analysis of the Hoekens straight-line mechanism is performed in Section 2. Then, in Section 3, a planar deployable mechanism consisting of Hoekens linkages is described, its singularities are analyzed, and the magnification ratio is computed. In Section 4, a procedure for combining the introduced DMs to form larger deployable structure is given, and a family of deployable mast units is obtained. Various prism DMs assembled using these mast units are described in Section 5. Section 6 discusses the optimal choice of the actuated joint. Finally, Section 7 analyzes the structural performance of the mechanism through simulation.

2. The straight-line mechanism

A straight-line mechanism produces (precise or approximate) straight-line output motion from an input element that rotates, oscillates, or moves in a straight line. Probably the best-known example is the straight-line mechanism developed by Watt for guiding the piston of early steam engines in 1784. Other well-known linkages are the Hoekens, the Chebyshev, and the Peaucellier–Lipkin linkages. Often, straight-line mechanisms have many links; only the Watt, the Evans, the Chebyshev, and the Hoekens are four-bars [12].

Compared to other linkages, the Hoekens has two advantages that make it more suitable as a unit mechanism of a DM. First, the configurations at the two ends of the straight-line motion are quite different, one compact, the other not, allowing a large magnification ratio. Second, the trajectory of the straight-line motion is “on one side” of the mechanism. This feature makes it easier to form a mechanism that can change its external profile in only one direction, and, using such mechanisms, compose a DM with constant sectional area and relatively few geometric constraints. For these reasons, in this work the Hoekens linkage is selected as a unit mechanism to compose a novel planar deployable mechanism. Its coupler can generate a partially straight point-path under the condition that the length ratio of the links is $l_1{:}l_2{:}l_3{:}l_4 = 2{:}1{:}2.5{:}2.5$. The Hoekens linkage and its coordinate system *OXYZ* are shown in Fig. 1. (The unit coordinate vectors will be denoted by $\vec{i}$, $\vec{j}$, $\vec{k}$.)

2.1. Position analysis

The reference configuration, where joint angles are set to zero, is shown in Fig. 1. Due to the given link–length ratios, special geometrical conditions exist, which make position kinematics of the linkage easier to solve than that of a more general four-bar. Because $l_3 = l_4$, there is always a right angle at *C* in the triangle ΔACP, Fig. 2. We use this to solve the kinematics of the Hoekens linkage.

The distance between point *A* and point *C* is

$$l_{AC} = \sqrt{l_{OA}^2 + l_{OC}^2 - 2l_{OA}l_{OC}\cos\left(\frac{\pi}{2} + \theta_1\right)} = l_2\sqrt{5 + 4\sin\theta_1}, \tag{1}$$

where θ_1 is the angular variable of the revolute joint at point *O*, l_{AC}, l_{OA}, and l_{OC} are the distances between the corresponding points, with $l_{OA} = l_2$ and $l_{OC} = l_1$.

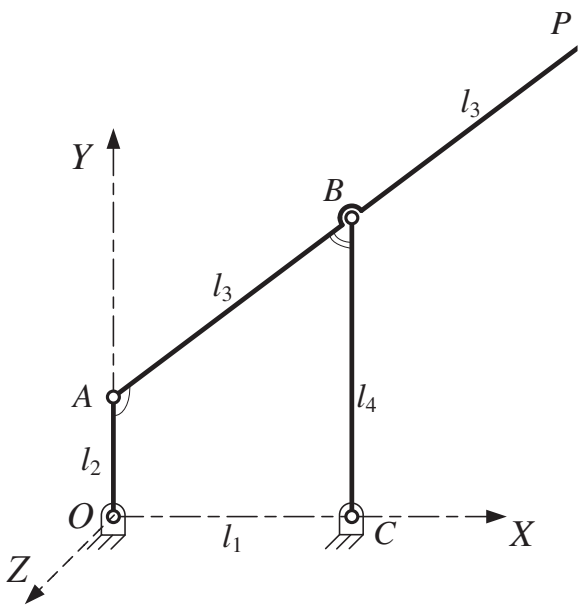

Fig. 1. The Hoekens linkage.

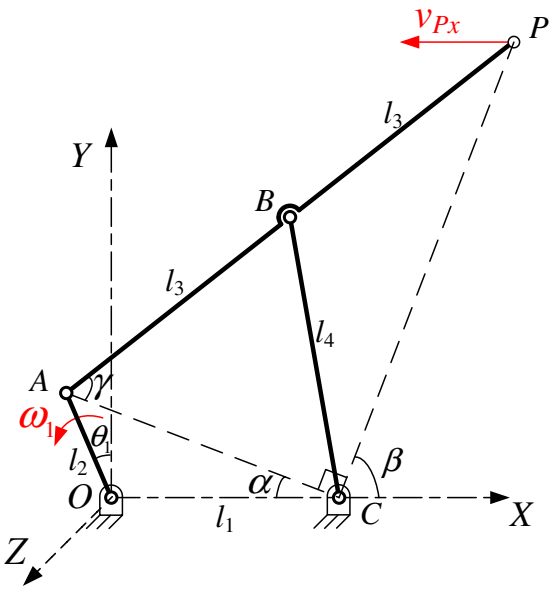

Fig. 2. Geometrical analysis of the Hoekens linkage.

The angle γ between AC and AP is

$$\gamma = \arccos\left(\frac{l_{AC}^2 + l_{BC}^2 - l_{AB}^2}{2l_{AC}l_{BC}}\right) = \arccos\left(\frac{1}{5}\sqrt{5 + 4\sin\theta_1}\right), \tag{2}$$

and so the distance between point P and point C is

$$l_{PC} = l_{AP}\sin\gamma = 2l_2\sqrt{5 - \sin\theta_1}. \tag{3}$$

The angle β, between PC and the x axis, complements angle α, between OC and AC, to a right angle.

$$\alpha = \arccos\left(\frac{l_{OC}^2 + l_{AC}^2 - l_{OA}^2}{2l_{OC}l_{AC}}\right) = \arccos\left(\frac{2 + \sin\theta_1}{\sqrt{5 + 4\sin\theta_1}}\right). \tag{4}$$

From the above equations, the position of the coupler point P is obtained,

$$x_P = x_c + l_{PC}\cos\beta = x_c + l_{PC}\sin\alpha = 2l_2 + 2l_2\frac{\sqrt{5 - \sin\theta_1}\cos\theta_1}{\sqrt{5 + 4\sin\theta_1}}, \tag{5}$$

$$y_P = l_{PC}\sin\beta = l_{PC}\cos\alpha = 2l_2\frac{\sqrt{5 - \sin\theta_1}(2 + \sin\theta_1)}{\sqrt{5 + 4\sin\theta_1}}. \tag{6}$$

The trajectory of point P in one motion cycle is shown in Fig. 3, with the length of the crank is $l_2 = 20$. When the crank rotates form 0° to 180°, point P moves nearly in a straight line from P_0 to P_{180} (the maximum deviation in the y direction is less than one percent of the length of the crank). In the following sections, the end effector point P is assumed to be performing a straight-line motion.

As the middle point of segment AP, the position of point B is

$$x_B = \frac{1}{2}(x_A + x_P) = l_2 + l_2\frac{\sqrt{5 - \sin\theta_1}\cos\theta_1}{\sqrt{5 + 4\sin\theta_1}} - \frac{1}{2}l_2\sin\theta_1, \tag{7}$$

$$y_B = \frac{1}{2}(y_A + y_P) = l_2\frac{\sqrt{5 - \sin\theta_1}(2 + \sin\theta_1)}{\sqrt{5 + 4\sin\theta_1}} + \frac{1}{2}l_2\cos\theta_1. \tag{8}$$

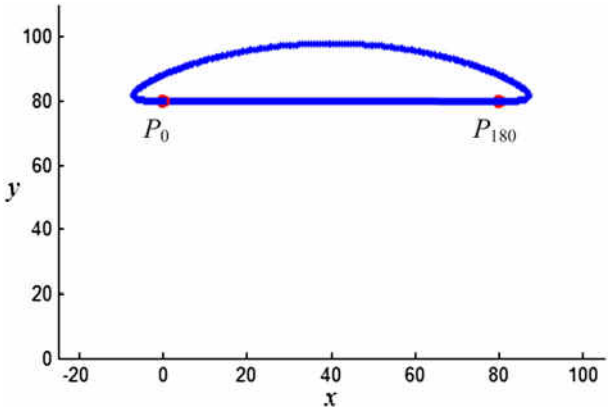

Fig. 3. The trajectory of point *P*.

2.2. Velocity analysis

We use screw theory [13,14] to obtain the velocity equations of the Hoekens linkage. The movement variables of the linkage are defined as shown in Fig. 4.

The planar twist of a revolute joint with axis through a point $Q = (x_Q, y_Q)$ and angular speed ω is

$$\boldsymbol{\rho} = \begin{bmatrix} \omega \\ \vec{v} \end{bmatrix} = \begin{bmatrix} \omega \\ v_x \\ v_y \end{bmatrix} = \omega \begin{bmatrix} 1 \\ y_Q \\ -x_Q \end{bmatrix}. \tag{9}$$

The closed-loop twist equation of the Hoekens linkage, which describes the instantaneous motion at any specific configuration, is

$$\omega_1\boldsymbol{\rho}_1 + \omega_2\boldsymbol{\rho}_2 + \omega_3\boldsymbol{\rho}_3 + \omega_4\boldsymbol{\rho}_4 = 0, \tag{10}$$

where $\omega_i = \dot{\theta}_i$ and $\boldsymbol{\rho}_i$, $i = 1, \ldots, 4$, are the joint speeds and the joint screws, respectively.

A "planar" wrench reciprocal to the joint-3 and joint-4 twists can be represented as a pure force with a line of action "in the plane of motion" intersecting the two joint axes, that is

$$\boldsymbol{\varphi}_{34} = \begin{bmatrix} m_{34} \\ \vec{f}_{34} \end{bmatrix} \tag{11}$$

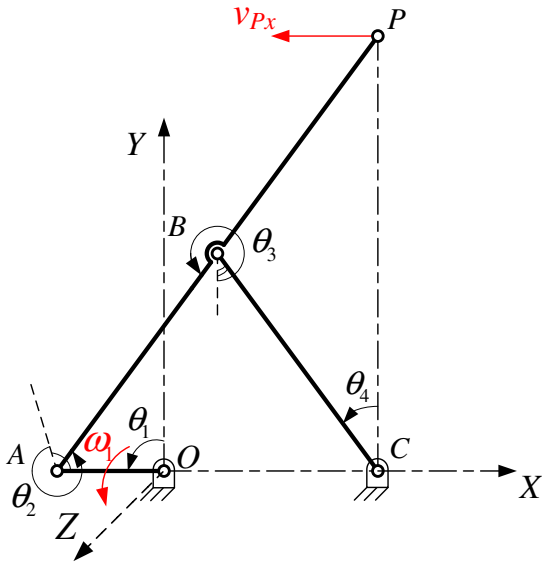

Fig. 4. Joint angle definitions of the Hoekens linkage.

where the force vector and moment are

$$\vec{f}_{34} = \begin{bmatrix} x_3 - x_4 \\ y_3 - y_4 \end{bmatrix} \tag{12}$$

and

$$m_{34} = l_1(y_3 - y_4) \tag{13}$$

respectively.

The passive joint velocities can be eliminated from the closed-loop twist equation by computing the reciprocal products of the left side by $\boldsymbol{\varphi}_{34}$, obtaining

$$\omega_1 \boldsymbol{\varphi}_{34} \cdot \boldsymbol{\rho}_1 + \omega_2 \boldsymbol{\varphi}_{34} \cdot \boldsymbol{\rho}_2 = 0. \tag{14}$$

Thus,

$$\omega_2 = -\frac{\boldsymbol{\varphi}_{34} \cdot \boldsymbol{\rho}_1}{\boldsymbol{\varphi}_{34} \cdot \boldsymbol{\rho}_2} \omega_1. \tag{15}$$

The reciprocal product measures the power, $\boldsymbol{\psi} \cdot \boldsymbol{\xi} = m\omega + \vec{f} \cdot \vec{v}$, exerted by a wrench $\boldsymbol{\psi} = [m, \vec{f}]^{\mathrm{T}}$ on a twist motion $\boldsymbol{\xi} = [\omega, \vec{v}]^{\mathrm{T}}$. The wrench and twist are called reciprocal if this power is zero. In the planar case, the product is proportional to the distance between the force and rotation axes, and so the denominator in (15) is never zero as points *A*, *B* and *C* are never aligned.

The end-effector twist, $\boldsymbol{\xi}_{AB}$, as the sum of the twists in joints 1 and 2 is

$$\boldsymbol{\xi}_{AB} = \omega_1 \boldsymbol{\rho}_1 + \omega_2 \boldsymbol{\rho}_2. \tag{16}$$

Then, the velocity of point *P* in the base frame is

$$\vec{v}_P = \omega_{AB} \vec{k} \times \overrightarrow{OP} + \vec{v}_{AB} \tag{17}$$

where ω_{AB} and $\vec{v}_{AB}$ are the angular and linear components of the twist $\boldsymbol{\xi}_{AB}$ respectively, i.e., the angular speed of the coupler and the velocity of its point instantaneously coincident with the origin. (In keeping with usual practice, we interpret the same notation, $\vec{v}$, depending on the context as either a 2×1 or 3×1 column matrix of components when the vector is in the *OXY* plane, i.e., $\vec{v} = v_x \vec{i} + v_y \vec{j}$.)

Fig. 5 plots the velocity of coupler point *P* in the *x* direction. It is easy to see that in the stage of straight-line motion, the motion of point *P* is approximately uniform. This characteristic ensures that the mechanism can have a stable motion while tracing a straight line.

2.3. Statics analysis

Given an external wrench, $\boldsymbol{\psi}_{AB}$, acting on the end-effector *AB* of the Hoekens linkage, a generalized force Θ_i, with corresponding generalized coordinate the input angle θ_i, is needed in order to maintain the configuration of the mechanism.

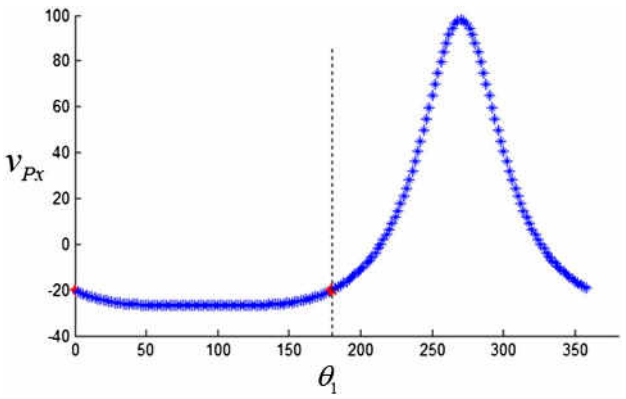

Fig. 5. The velocity of point *P* in the *x* direction.

Based on the *principle of virtual work*, the relationship between the wrench and the generalized force is

$$\Theta_i \omega_i = \boldsymbol{\psi}_{AB} \cdot \boldsymbol{\xi}_{AB} \tag{18}$$

where ω_i is the input joint speed and $\boldsymbol{\xi}_{AB}$ is the twist of the end-effector.

If the twist is a rotation and the external wrench is a pure force with magnitude f, Fig. 6, we have

$$\Theta_i \omega_i = \boldsymbol{\psi}_{AB} \cdot \boldsymbol{\xi}_{AB} = m_Q \omega = \left(\vec{d}_\perp \times \vec{f}\right) \cdot \vec{k}\omega = \varepsilon d_\perp f \omega. \tag{19}$$

In Eq. (19), m_Q is the moment of the force with respect to the instantaneous center of rotation, $d_\perp$ is the distance between the axes of the force and rotation. The sign $\varepsilon = \mathrm{sgn}\left(\vec{d}_\perp \times \vec{f} \cdot \vec{k}\right)$, where $\vec{d}_\perp$ is from the instantaneous center to the force axis, is positive when the force attempts to turn the body counterclockwise (it is -1 in the figure).

Thus, the required generalized force is

$$\Theta_i = \varepsilon \frac{\omega_o}{\omega_i} f d_\perp. \tag{20}$$

The Jacobian matrix, J, can be used to relate the actuated generalized force to end-effector wrenches [14]. If the relation between ω_i and end-effector twist $\boldsymbol{\xi}_{AB}$ is

$$\boldsymbol{\xi}_{AB} = J\omega_i, \tag{21}$$

we have

$$\Theta_i \omega_i = \boldsymbol{\psi}_{AB} \cdot \boldsymbol{\xi}_{AB} = \boldsymbol{\psi}_{AB} \cdot J\omega_i = J^T \boldsymbol{\psi}_{AB} \omega_i \tag{22}$$

for any ω_i. Therefore,

$$\Theta_i = J^T \boldsymbol{\psi}_{AB}, \tag{23}$$

where J is the Jacobian matrix describing the relationship between the input variable and the output velocity.

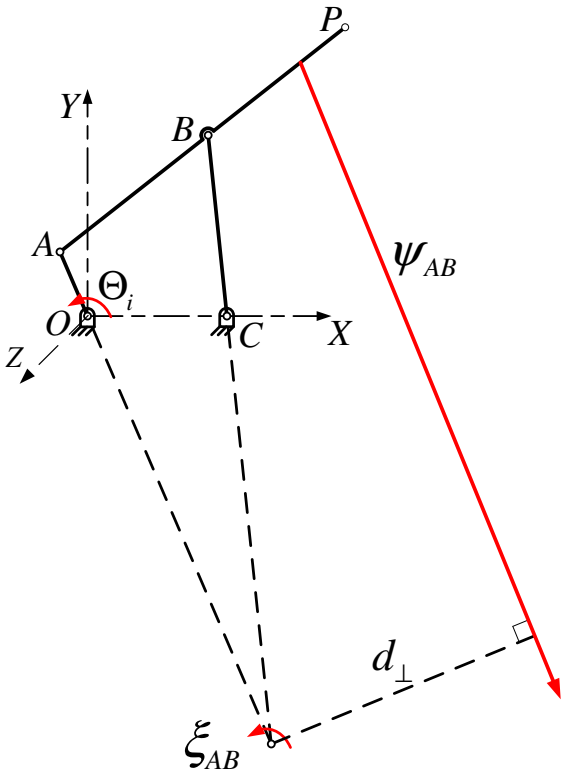

Fig. 6. Output twist and external wrench at the end-effector.

Considering the four-bar linkage as a parallel mechanism with the coupler as the moving platform, there are two legs from the base to the end-effector, joints 1 and 2, and joints 4 and 3, respectively. The end-effector twist, $\boldsymbol{\xi}_{AB}$, can also be expressed as the sum of the twists in joints 4 and 3,

$$\boldsymbol{\xi}_{AB} = \omega_4 \boldsymbol{\rho}_4 + \omega_3 \boldsymbol{\rho}_3. \tag{24}$$

As mentioned in the last subsection, once the wrench, $\boldsymbol{\varphi}_{21}$, which is reciprocal to the joint-1 and joint-2 twists is known, the relationship between ω_4 and ω_3 can be obtained through the reciprocal product between $\boldsymbol{\varphi}_{21}$ and the closed-loop twist equation.

The wrench reciprocal to the joint-1 and joint-2 screws is a pure force with axis intersecting the two revolute-joint axes, that is

$$\boldsymbol{\varphi}_{21} = \begin{bmatrix} m_{21} \\ \vec{f}_{21} \end{bmatrix} \tag{25}$$

where the force vector and moment are

$$\vec{f}_{21} = \begin{bmatrix} x_2 - x_1 \\ y_2 - y_1 \end{bmatrix} \tag{26}$$

and

$$m_{21} = 0 \tag{27}$$

respectively.

By left-multiplication of Eq. (10) with $\boldsymbol{\varphi}_{21}$, the passive joint velocities of joint 1 and 2 are eliminated. The obtained relationship between the velocities of joints 3 and 4 is

$$\omega_3 = -\frac{\boldsymbol{\varphi}_{21} \cdot \boldsymbol{\rho}_4}{\boldsymbol{\varphi}_{21} \cdot \boldsymbol{\rho}_3} \omega_4. \tag{28}$$

By substituting Eq. (28) into Eq. (24) and Eq. (15) into Eq. (16), the Jacobian matrices corresponding to different joints are obtained

$$J_a = \boldsymbol{\rho}_a - \frac{\boldsymbol{\varphi}_{cd} \cdot \boldsymbol{\rho}_a}{\boldsymbol{\varphi}_{cd} \cdot \boldsymbol{\rho}_b} \boldsymbol{\rho}_b \tag{29}$$

where a, b, c, and d label the four joints of the linkage, a and b belonging to one leg, and c and d to the other, $\{(a, b), (c, d)\} = \{(1,2), (3,4)\}$.

By substituting Eq. (29) into Eq. (23), the required torque at each joint is obtained

$$\Theta_a = \left[\boldsymbol{\rho}_a - \frac{\boldsymbol{\varphi}_{cd} \cdot \boldsymbol{\rho}_a}{\boldsymbol{\varphi}_{cd} \cdot \boldsymbol{\rho}_b} \boldsymbol{\rho}_b \right]^{\mathrm{T}} \boldsymbol{\psi}_{AB}. \tag{30}$$

It can be seen from Eq. (30) that if $\boldsymbol{\varphi}_{cd} \cdot \boldsymbol{\rho}_b = 0$ the relationship between the end-effector wrench and the joint torque degenerates. This happens in a singular configuration when the centers of the three passive joints, b, c, and d, are aligned. Singularities are discussed in Section 3.2.

3. A planar deployable mechanism based on the Hoekens straight-line linkage

The kinematic properties of the Hoekens linkage, analyzed above, make it possible to construct a novel planar deployable mechanism (PDM) composed of four straight-line linkages. The coupler points of the PDMs are used to form a rectangle which can expand in only one dimension.

3.1. Structure of the planar deployable mechanism

The novel planar deployable mechanism is shown in Fig. 7. The four Hoekens linkages share a common base $C_{13}C_{24}$. Linkage $O'A_1B_1C_{13}$ and linkage $O'A_2B_2C_{24}$ share the common crank A_1A_2, while linkage $O'A_3B_3C_{13}$ and linkage $O'A_4B_4C_{24}$ share the common crank A_3A_4. Therefore, the coupler points P_1 and P_2 move together, and so do P_3 and P_4. Crank A_1A_2 and crank A_3A_4 are rotating around the common point O'. The coordinate system of the planar deployable mechanism is described in Fig. 7. In the initial configuration, P_1 and P_3 have the same Y coordinate.

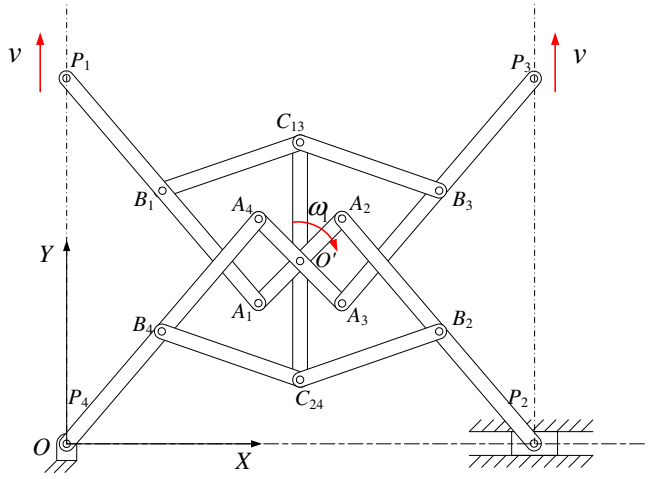

Fig. 7. A planar deployable mechanism based on the Hoekens linkage.

Essentially, the planar deployable mechanism is formed by two groups of Hoekens linkages sharing a common link, thus the DOF of the assembly is two. This agrees with the general Chebyshev–Grübler–Kutzbach formula, as the assembly has 11 links and 14 revolute joints, and the predicted degree of freedom is

$$M = d(n-g-1) + \sum_{i=1}^{g} f_i = 3(11-14-1) + 14 = 2 \tag{31}$$

where d is the order of the system, n is the number of the links including the base, g is the number of joints and f_i is the number of degrees of freedom for the i-th joint.

To obtain a one-DOF mechanism, which is convenient for actuation and control, crank A_1A_2 and crank A_3A_4 are connected via two pairs of bevel gear, Fig. 8. Since the transmission ratio of each bevel gear is $\mu = 1$, the two cranks are constrained to rotate with the same angular velocity and in opposite directions.

We distinguish three representative configurations of the PDM: the completely folded configuration, the middle configuration, and the completely deployed configuration. From the kinematics of the Hoekens linkage, when the angle of crank A_1A_2 is in the range of 0° to 180°, the rectangle formed by the four coupler points is folded in only one dimension (along the Y axis in Fig. 7), while the size of its other side remains the same.

When the mechanism is in the folded configuration, the coupler points of the four Hoekens linkages merge into two points, $P_1 = P_4$ and $P_2 = P_3$. With the rotation of the cranks, two coupler points, P_1 and P_3, move up along two straight lines perpendicular to the base, while distance between the two lines remains invariant. The velocities of the two points remain the same during the motion,

$$\vec{v}_{P1} = \vec{v}_{P3}. \tag{32}$$

The deployment process of the PDM is shown in Fig. 9.

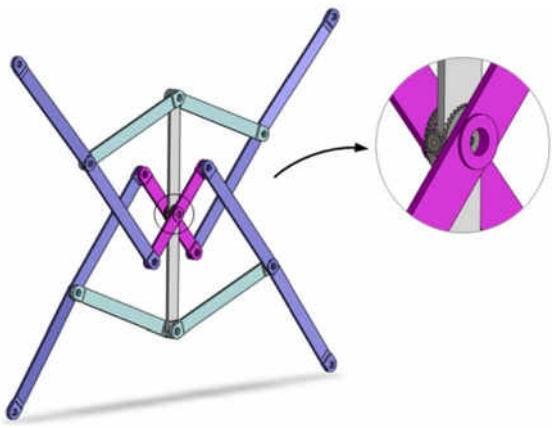

Fig. 8. Gear connection between the two cranks.

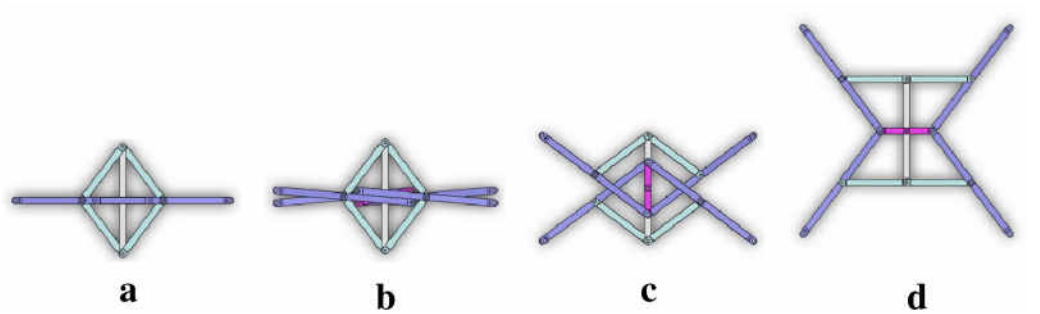

Fig. 9. Deployment process of the mechanism.

3.2. Singularity analysis of the planar deployable mechanism

Because the basic unit of the planar deployable mechanisms is a four-bar linkage, singularities can be expected. The constituent four Hoekens linkages perform the same motion at the same time, and so the singularity of one Hoekens linkage will coincide with the singularities of the others. Therefore, it is sufficient to analyze only one straight-line linkage unit.

A configuration is nonsingular when the mechanism's velocity state can be completely determined both from the input velocity and from the output velocity [15]. Since we are interested in the velocity of point P along its straight-line path, it is natural to interpret $\dot{x}_P$ as the instantaneous output. The input velocity should be the speed of one of the joints fixed at the base of the four-bar, ω_1 or ω_4.

The forward kinematics of a four-bar becomes singular if and only if the three passive-joint centers become aligned. Indeed, if we take θ_4 as the actuated joint, from Eq. (10) we have

$$\dot{\theta}_4\boldsymbol{\rho}_4 = [\,-\boldsymbol{\rho}_1 \quad -\boldsymbol{\rho}_2 \quad -\boldsymbol{\rho}_3\,]\begin{bmatrix}\dot{\theta}_1\\ \dot{\theta}_2\\ \dot{\theta}_3\end{bmatrix} = \begin{bmatrix} 0 & -l_2\cos\theta_1 & -l_4\cos\theta_4\\ 0 & -l_2\sin\theta_1 & -l_4\sin\theta_4 + l_1\\ -1 & -1 & -1\end{bmatrix}\begin{bmatrix}\dot{\theta}_1\\ \dot{\theta}_2\\ \dot{\theta}_3\end{bmatrix}. \tag{33}$$

Given ω_4, the velocity state of the mechanism is indeterminate if and only if the 3×3 matrix in Eq. (33) is singular, i.e., when the three unactuated-joint screw axes are coplanar. It is easy to see that this happens in two configurations, given by $\theta_1 = 180°$and $\theta_1 = 314.39°$. These two singularities belong to the Impossible Input (II) type [15]: the input joint is blocked (because its joint screw is not in the span of the other three), and also of the Redundant Output (RO) type: the output link (the coupler AP) cannot be controlled and point P can have a velocity with a nonzero projection on the x axis [15]. The two singular (RO, II) configurations relevant to the PDM are shown in Fig. 10.

The first one, in Fig. 10(a), is the completely folded configuration of the PDM. Links A_1A_2, A_1B_1, A_2B_2, A_3A_4, A_3B_3, and A_4B_4 overlap. From the kinematic analysis, it follows that the second solution is out of the range of the straight-line motion (and also not in the category of unchanged cross section of the mechanisms to be proposed in the following sections).

Switching the input joint changes the singular configurations of the mechanism. If the actuated joint is θ_1, Eq. (10) yields

$$\dot{\theta}_1\boldsymbol{\rho}_1 = [\,-\boldsymbol{\rho}_2 \quad -\boldsymbol{\rho}_3 \quad -\boldsymbol{\rho}_4\,]\begin{bmatrix}\dot{\theta}_2\\ \dot{\theta}_3\\ \dot{\theta}_4\end{bmatrix} = \begin{bmatrix} -l_2\cos\theta_1 & 0 & -l_4\cos\theta_4\\ -l_2\sin\theta_1 & l_1 & -l_4\sin\theta_4 + l_1\\ -1 & -1 & -1\end{bmatrix}\begin{bmatrix}\dot{\theta}_2\\ \dot{\theta}_3\\ \dot{\theta}_4\end{bmatrix}. \tag{34}$$

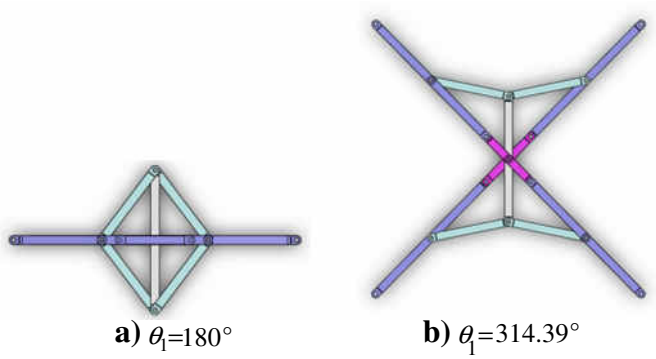

Fig. 10. Singularities of the PDM.

In this case, the three-screws matrix will never lose rank, as points *A*, *B*, and *C* cannot be aligned. (Because the triangle inequalities cannot be satisfied; the linkage is strictly Grashof and link *OA* is the crank.) Therefore, there is no input (forward-kinematics) singularity when θ_1 is actuated.

The inverse kinematics is singular if and only if the output velocity is necessarily zero. (The only alternative would be a configuration of Increased Instantaneous Mobility, IIM see [15], with all four joint screws coplanar, not possible for this four-bar. Indeed, if there is one instantaneous dof, a non-zero projection of the velocity of any point of the coupler determines all velocities.) Point *P* is never stationary because it can never coincide with the instantaneous center of the coupler as it cannot be collinear both with *O*, *A*, and with *B*, *C*. If $\dot{x}_P$ is considered as the instantaneous output, the mechanism has configurations of Impossible Output (and Redundant Input) where the projection of point *P* on the *x* axis reverses direction, but these configurations are just outside the straight-line-motion range, Fig. 3.

3.3. Magnification ratio with respect to link shape

The kinematics and singularity analysis performed above is based on the assumption that motion is never hindered by link interference. In fact, the links need to have some physical shapes and it is difficult for a practical design to ensure interference-free motion (e.g. by having links move in distinct planes). Thus, it is reasonable to assume that P_2 and P_3 cannot coincide, and, in practice, the maximally folded configuration will bring P_2 and P_3 as close as possible, Fig. 11.

Accordingly, the magnification ratio *r* is defined as

$$r = \frac{l_{\max}}{l_{\min}} \tag{35}$$

where $l_{\max}$ is the distance between point P_2 and point P_3 in the completely deployed configuration, while $l_{\min}$ is measured between point P_2 and point P_3 in the maximally folded configuration.

For a practical planar deployable mechanism, which exactly is the maximally folded configuration, it will depend on the physical geometry of the links. According to the kinematic analysis, the two output links connected with the same crank remain parallel with each other during the motion. So, the configuration where these two links come in contact is called completely folded, Fig. 11.

In this configuration, the angle between link A_1A_2 and link A_2P_2 can be obtained as

$$\sin\theta_2' = \frac{d}{l_2}, \tag{36}$$

where *d* is the width of the output link A_2P_2, l_2 is the length of link A_1A_2, and θ_2' is the angle between link A_2P_2 and link A_1A_2. The distance $l_{\min}$ can be obtained by substituting θ_2' into Eq. (5).

When $\theta_1 = 0°$, the mechanism is located at the limit of the straight-line motion range, and this configuration is called completely deployed, thus $l_{\max} = 4l_2$.

Fig. 12 shows how the magnification ratio changes with the width of the output link when the latter ranges from $0.1l_2$ to $0.5l_2$. It can be seen that the magnification ratio decreases with the increase of the output link's width, and that it decreases quickly in the initial stage.

4. The Hoekens rectangle as a unit mechanism

Herein we discuss briefly the principles of assembling a large deployable mechanism with one degree of freedom and apply them to the Hoekens-linkage-based rectangle. A typical design objective is for the deployed combined structure to have a desired shape.

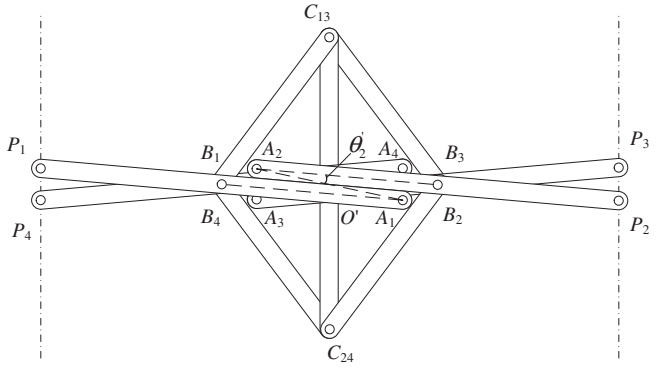

Fig. 11. Maximally folded configuration in practice.

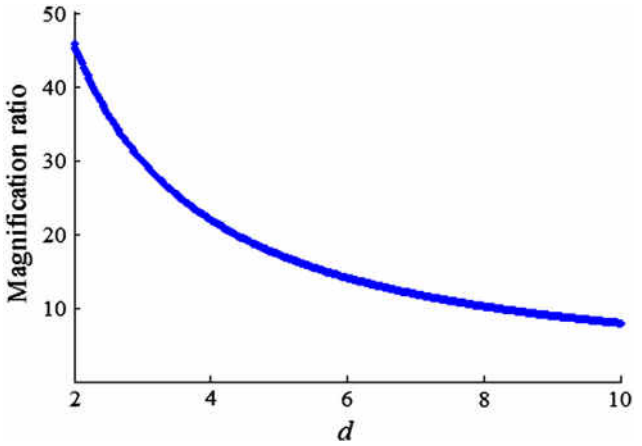

Fig. 12. The magnification ratio, *r*, as a function of the width of the output link, *d*.

4.1. Principles of combining unit mechanisms

A deployable mechanism is made up of a number of primary mechanism units. Every two mechanism units are able to combine with each other while remaining movable. In order to guarantee that the mechanical assembly with infinitely many unit mechanisms still has a finite degree of freedom, and can form a desired deployed shape, the following general conditions need to be satisfied,

(1) At a certain configuration, the unit mechanism can be assembled to form the desired shape while satisfying all geometric constraints.
(2) The assembly is able to move, and geometric constraints are still satisfied when the assembly undergoes an arbitrary small motion.
(3) The addition of a new unit will not increase the degree of freedom.

Conditions (1) and (2) guarantee that the combined mechanism is still a movable assembly under the given geometric constraints, while Condition (3) ensures that units can be added infinitely.

4.2. Deployable mast unit

Based on the above principles, the deployable planar linkages can be assembled in order to obtain a desired shape. A planar assembly of two PDMs directly hinged at two superimposed points is shown in Fig. 13. The end effectors of the two PDMs, points P'_1, P_3, P_2, and P'_4, form a big rectangle. The position and speed of the output points P'_1 and P_3 remain the same during the motion. The mobility of the planar assembly is one. All the conditions of assembly are satisfied and so the combination of PDMs with hinges at the end effector points is valid.

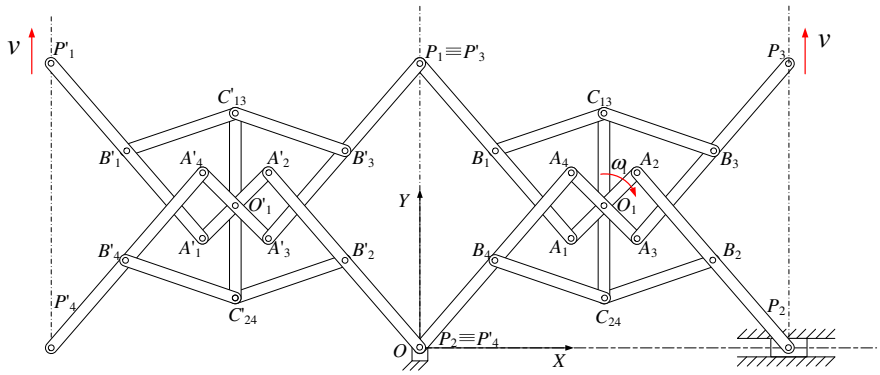

Fig. 13. A planar assembly consisting of two PDMs.

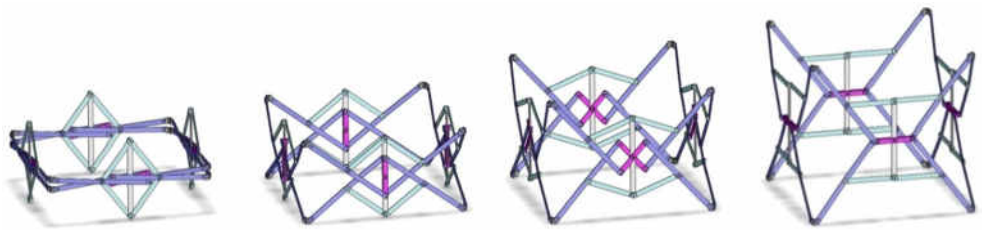

Fig. 14. Deployment process of a square deployable mast unit.

The combination can also be expanded into space, if the common revolute joint is replaced by the two revolute joints whose axes are normal to the plane of each PDM. The angle between the two axes depends on the shape of the cross section,

$$\varphi = \frac{360^{\circ}}{n_e} \tag{37}$$

where n_e is the number of edges of the cross-section regular polygon.

A triangular mast unit and a square mast unit, built out of planar deployable linkages, are shown in Figs. 13–14 and 15–16, respectively. The triangular mast unit has three PDMs and the square mast unit has four PDMs. The masts can be deployed and folded through the rotation of the crank. The adjacent PDMs are connected with a corner part with two revolute joints, and the rotation axis is normal to the plane of each PDM. In each case, the obtained mechanism performs a continuous movement with only one degree of freedom, and the cross section remains constant, as shown in Fig. 15 and Fig. 17.

5. Deployable prism mechanism assembled with deployable mast units

In this section, we describe a deployable prism mechanism which consists of mast units of the type described in the previous section. Connection between adjacent units is investigated, and a kinematic simulation is performed.

As explained in the previous sections, all the vertices of the mast unit are moved along a direction perpendicular to the cross section. The deployable mast unit can be assembled to form a large deployable mechanism along the deployment direction by fixing the corner parts together. However, the mast unit is able to move in only one direction, and the rotating motion of the output link cannot be transferred from one unit to an adjacent one. Thus, the DOF will be increased while adding new units. Gears or a crank-slider mechanism can be used to transmit the motion while maintaining the degree of freedom, Figs. 18 and 19.

In order to show the movement of the mechanism clearly, the spur gear has been chosen as a transmission component in the following analysis, the end of two output links of the PDMs are engaged through it, as shown in Fig. 19(a). The solid model of the combination of PDMs is illustrated in Fig. 19(b) and Fig. 19(c).

By fixing their corners together and connecting them with the spur gear, PDM mast units can be assembled into a larger prism deployable mechanism along the deployment direction. The DOF of the obtained mechanism remains one. This deployable mechanism was designed and simulated with Solidworks, Fig. 20. The simulated DM is assembled with three mast units. The single rotation input is at the revolute joint in the center of one PDM in the lowest mast unit. Fig. 20(a) shows the folded

Fig. 15. Cross section of a square deployable mast unit.

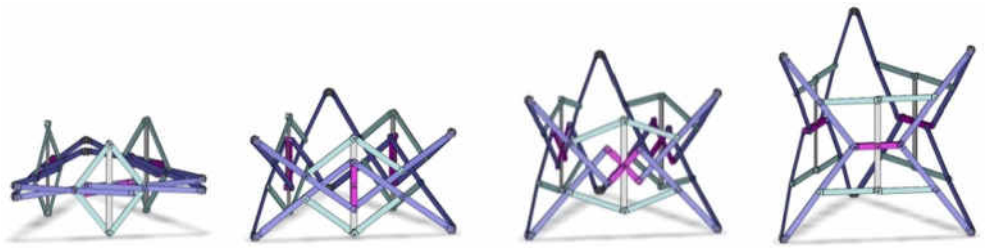

Fig. 16. Deployment process of a triangular deployable mast unit.

configuration, and the completely deployed configuration is in Fig. 20(c). The simulation confirms that the mobility of this assembled deployable mechanism is indeed one.

However, if the mast units have the same cross section, the combined mechanism cannot be completely folded due to the physical shape of the link $C_{13}C_{24}$, as shown in Fig. 20(a). This problem can be solved by using deployable mast units with slightly different cross section areas. The units are then able to overlap, forming a telescopic mast, Fig. 21.

By combining the deployable units in this way, the magnification ratio of the prism deployable mechanism is increased significantly. The deployed length of the prism mechanism with n mast units is

$$h_{\max} = 2nl_{21} + n(n-1)\Delta l \tag{38}$$

where l_{21} is the length of link A_1A_2 of the innermost mast unit, and Δl is the length change of link A_1A_2 between adjacent units.

The corresponding folded length is

$$h_{\min} = l_{21} - l_{\min 1} + l_{2n} - l_{\min n} + \sum_{i=1}^{n} l_{\min i} \tag{39}$$

where l_{2n} is the length of link A_1A_2 of the outermost mast unit, and $l_{\min i}$ is the distance between points P_2 and P_3 in the folded configuration of the i-th mast unit.

Therefore, the magnification ratio r_n considering the geometric shape of link $C_{13}C_{24}$ is,

$$r_n = \frac{h_{\max}}{h_{\min}}. \tag{40}$$

Furthermore, when increasing the number of units, n, the magnification ratio of the deployable prism mechanism, r_n, will be closer to that of the planar deployable mechanism, r, calculated in Section 3.

6. Choice of actuator

As the deployable prism mechanism proposed above has one degree of freedom, one actuator is sufficient to drive it. The location of the actuator is discussed in this section. Due to the fact that the deployment process involves low speeds and

Fig. 17. Cross section of a triangular deployable mast unit.

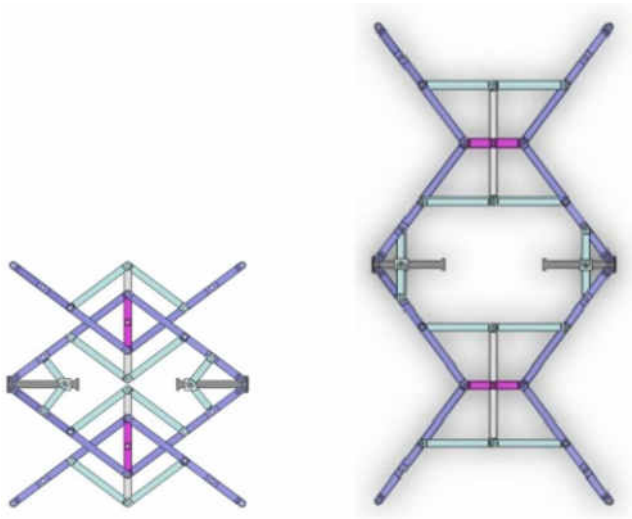

a) Folded configuration **b)** Deployed configuration

Fig. 18. Combination of two PDMs through a crank-slider mechanism.

accelerations, it is acceptable to use static-load analysis for the choice of the actuator. Reciprocal screws are used to eliminate the passive velocity in the closed loop twist equation.

The three revolutes in the central link $C_{13}C_{24}$, Fig. 22, are considered as actuated-joint candidates. During the mechanism motion cycle, their joint centers move along the same vertical line in the *OXY* plane.

Since the aim of this section is to choose the best location of the actuator, a comparison among the different locations is needed. The evaluation indexes are the magnitude and the stability of the driving torque. The following assumptions are made:

1. Each link of the prism deployable mechanism is a rigid bar with constant form during the movement;
2. Friction is ignored and joints are considered ideal;
3. The deployment speed is quite slow;
4. The gravity of links and joints of the base mast are ignored.

Based on the above assumptions, nearly all the force acting on the deployable mechanism is the gravity of the upper units and the load, and most of the driving force/torque is used to balance the gravity of the system. For this reason, the static analysis is sufficient to derive the actuating force/torque and it can be assumed that the mechanism is always in equilibrium.

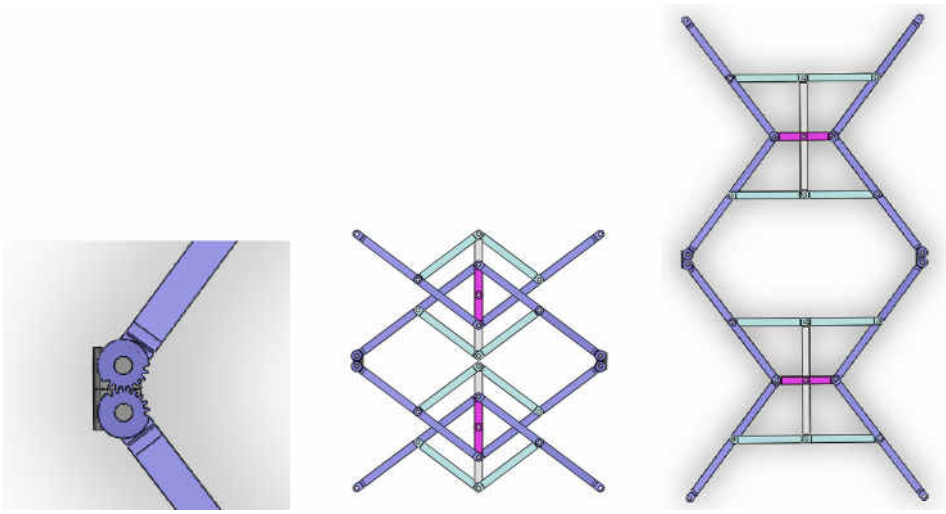

a) Spur gear transmission **b)** Folded configuration **c)** Deployed configuration

Fig. 19. Combination of two PDMs through a spur gear.

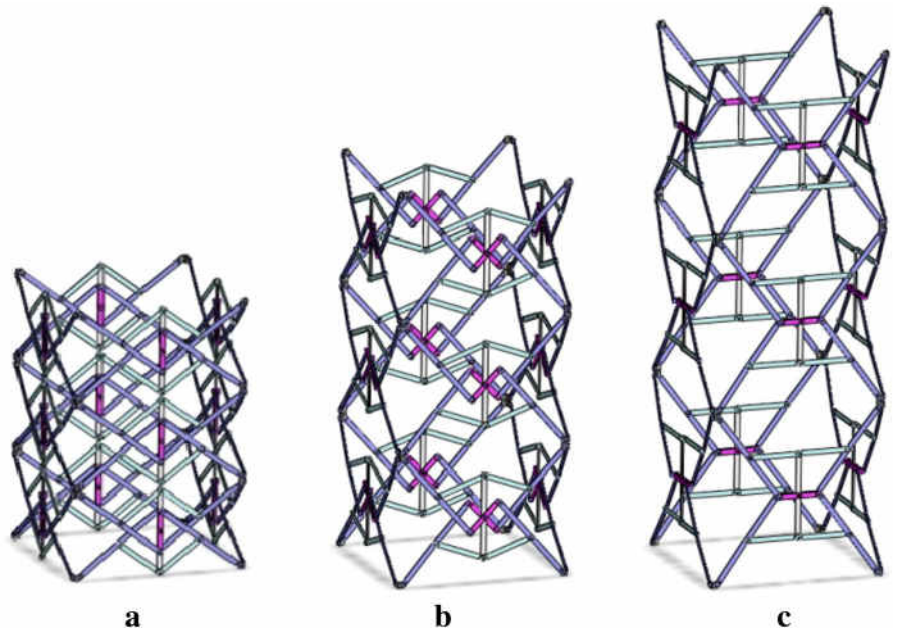

Fig. 20. Prism mechanism with a square mast unit t.

The two central links of the PDM are connected through a bevel gear, and so the magnitude of movement and driving torque are the same, and their directions are opposite. So, it is enough to solve the statics only considering the right-hand half of the mechanism. A prismatic joint is added in point O' to keep the motion of the end effector P_3, Fig. 23.

As derived in Section 2.3, the actuated torque (generalized force corresponding to the input joint), Θ_i, applied to the actuator to balance the external force of the deployable mast can be expressed as

$$\Theta_i = J_{P3}^T \boldsymbol{\varphi}_{P3} \tag{41}$$

where J_{P3} is the Jacobian matrix mapping the input variable, ω_i, into the output twist, $\boldsymbol{\xi}_{A3P3}$, of the end effector, while $\boldsymbol{\varphi}_{P3}$ is the force acting on the end effector.

The relation between ω_i and $\boldsymbol{\xi}_{A3P3}$ is

$$\boldsymbol{\xi}_{A3P3} = J_{P3}\omega_i \tag{42}$$

where ω_i is the joint velocity.

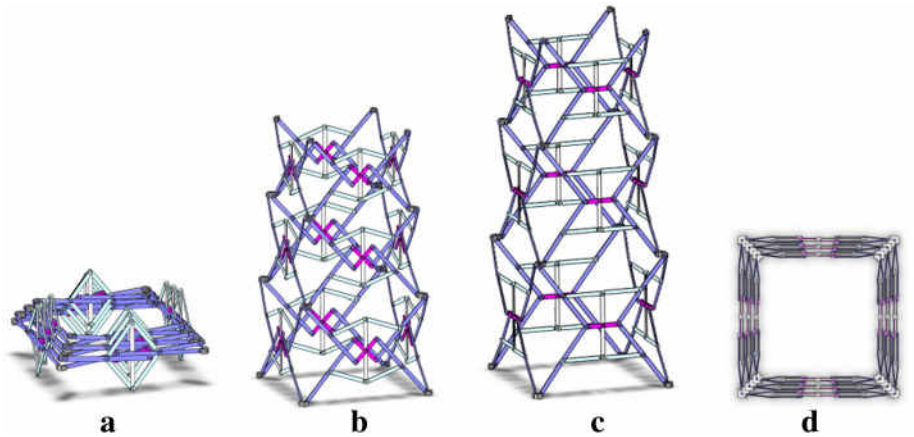

Fig. 21. Deployment of a telescopic mast.

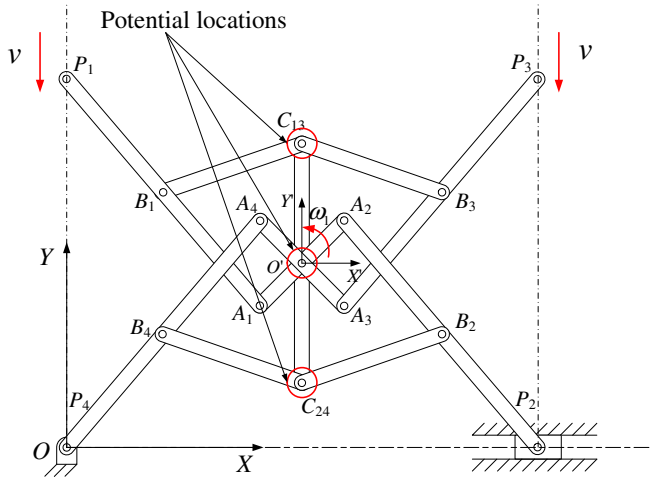

Fig. 22. Potential actuator locations.

It can be seen from Fig. 23 that the twist of the end-effector can be described as the sum of the twists in two serial chains,

$$\begin{aligned}\boldsymbol{\xi}_{A3P3} &= \omega_{P4}\boldsymbol{\rho}_{P4} + \omega_{A4}\boldsymbol{\rho}_{A4} + \omega_{A3}\boldsymbol{\rho}_{A3} \\ &= \omega_{P4}\boldsymbol{\rho}_{P4} + \omega_{B4}\boldsymbol{\rho}_{B4} + \omega_{C24}\boldsymbol{\rho}_{C24} + \omega_{C13}\boldsymbol{\rho}_{C13} + \omega_{B3}\boldsymbol{\rho}_{B3}.\end{aligned} \tag{43}$$

As an assembly of Hoekens linkages, the angles shown in Fig. 23 are linear functions of the angles in Section 2.2: $\omega_{P4} = \omega_1 + \omega_2$, $\omega_{A4} = \omega_2$, $\omega_{A3} = -\omega_2$, $\omega_{P4} = \omega_3 + \omega_4$, $\omega_{B4} = \omega_3$, $\omega_{C24} = \omega_4$, $\omega_{C13} = -\omega_4$, and $\omega_{B3} = -\omega_3$, where $\omega_i \quad i = 1, 2, 3, 4$ are the joint velocities of the Hoekens linkage.

Eq. (44) yields

$$\begin{aligned}\boldsymbol{\xi}_{A3P3} &= \omega_1\boldsymbol{\rho}_{P4} + \omega_2(\boldsymbol{\rho}_{P4} + \boldsymbol{\rho}_{A4} - \boldsymbol{\rho}_{A3}) \\ &= \omega_1\left(\boldsymbol{\rho}_{P4} - \frac{\boldsymbol{\varphi}_{34}\cdot\boldsymbol{\rho}_1}{\boldsymbol{\varphi}_{34}\cdot\boldsymbol{\rho}_2}(\boldsymbol{\rho}_{P4} + \boldsymbol{\rho}_{A4} - \boldsymbol{\rho}_{A3})\right)\end{aligned} \tag{44}$$

where ω_2 has been eliminated using Eq. (15).

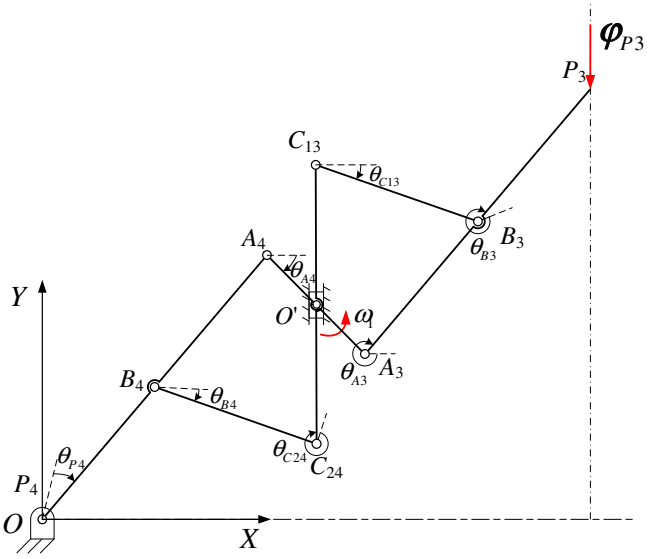

Fig. 23. Equivalent structural diagram.

Similarly,

$$\begin{aligned}\boldsymbol{\xi}_{A3P3} &= \omega_4(\boldsymbol{\rho}_{P4}+\boldsymbol{\rho}_{C24}-\boldsymbol{\rho}_{C13})+\omega_3(\boldsymbol{\rho}_{P4}+\boldsymbol{\rho}_{B4}-\boldsymbol{\rho}_{B3})\\ &= \omega_4\left(\boldsymbol{\rho}_{P4}+\boldsymbol{\rho}_{C24}-\boldsymbol{\rho}_{C13}-\frac{\boldsymbol{\varphi}_{21}\cdot\boldsymbol{\rho}_4}{\boldsymbol{\varphi}_{21}\cdot\boldsymbol{\rho}_3}(\boldsymbol{\rho}_{P4}+\boldsymbol{\rho}_{B4}-\boldsymbol{\rho}_{B3})\right)\end{aligned} \tag{45}$$

where ω_3 has been substituted from Eq. (28).

Using the corresponding relationship between the joint variables of the deployable unit and that of the Hoekens linkage, the end effector twist $\boldsymbol{\xi}_{A3P3}$ can be expressed as a function of joint velocity ω_i of the four-bar:

$$\boldsymbol{\xi}_{A3P3} = \begin{bmatrix} 1-\dfrac{2y_B}{M} \\ \dfrac{4y_Bx_A}{M} \\ -\dfrac{4y_By_A}{M} \end{bmatrix}\omega_1 = J_1\omega_1 \tag{46}$$

where $M = x_B\cos\theta_1 - 2l_2\cos\theta_1 + y_B\sin\theta_1 + 2y_B$, while x_A, y_A, y_B, indicate the coordinates of points A and B, Fig. 2.

Similarly, $\boldsymbol{\xi}_{A3P3}$ is a function of ω_4,

$$\boldsymbol{\xi}_{A3P3} = \begin{bmatrix} 1-\dfrac{2l_2\cos\theta}{L} \\ -2l_2+\dfrac{4l_2x_B\cos\theta_1}{L} \\ -\dfrac{4l_2y_B\cos\theta}{L} \end{bmatrix}\omega_4 = J_4\omega_4 \tag{47}$$

where $L = y_B\sin\theta_1 + x_B\cos\theta_1$.

The applied force at P_3 can be related to the joint torque by using the transpose of the Jacobian matrix

$$\Theta_1 = J_1^T\boldsymbol{\varphi}_{P3}, \tag{48}$$

$$\Theta_4 = J_4^T\boldsymbol{\varphi}_{P3}. \tag{49}$$

Here, the force applied at the end-effector is the gravity of the upper units of the deployable mast

$$\boldsymbol{\varphi}_{P3} = F_{P3}[0 \quad -1 \quad x_{P3}]^{\mathrm{T}} \tag{50}$$

where F_{P3} is the weight of the upper units, and x_{P3} is the projection of point P_3 on the x axis.

If the values of the parameters are $l_1 = 0.2$ m, $l_2 = 0.1$ m, $l_3 = 0.25$ m, $l_4 = 0.25$ m, and $F_{P3} = 200$ N, the actuating torques of joint 1 and joint 4 for the whole deployment circle are shown in Fig. 24.

The actuating torque of the joints is displayed in different colors. It can be seen that, the actuating torque of joint 4 grows at a steady rate in the initial stage, but because of the singularity, the value increases sharply when the rotation angle of crank A_1A_2 approaches 180°. However, this phenomenon does not occur when the actuator is placed at joint 1. The required actuated torque

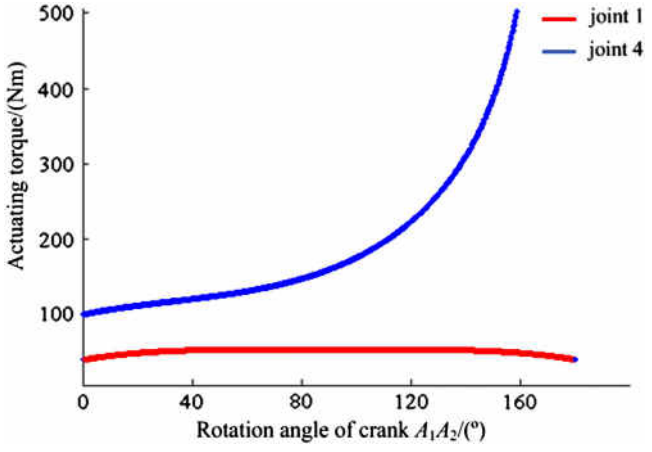

Fig. 24. Actuating torque at the two alternative active joints.

of joint 1 is much smaller on average, and much more stable, than that of joint 4. Clearly, joint 1 at O' in Fig. 22 is more suitable to be actuated.

7. Static structural stiffness and natural frequency of the deployable mechanism

Stiffness analysis is an engineering method that determines the deformation in material and structures subjected to forces or load. Normally, the deployable mast is working under a static force. Therefore, the stiffness analysis of the mechanism is focused on the static stiffness in this section. Natural frequency of the mechanism has also been analyzed in ANSYS. The results show that the proposed deployable mechanism can be used in practice, and some optimizing suggestions are given.

7.1. Modelling

The square deployable mast has been selected for analysis. The main parameters of the analyzed model are as follows: the number of unit is 3, the edge length of the cross section of the base unit is 1086 mm, that of the top unit is 886 mm, the height of the deployable mechanism is 2735 mm, and the width and thickness of the link are 30 mm and 5 mm, respectively. We suppose that all the links use the same material, the density is $p = 7.8 \times 10^3$ kg/m^3, and the Young's modulus of elasticity and the Poisson's ratio are 2.6×10^6 MPa and 0.31, respectively.

Several constraints are applied to the base in order to perform the finite element analysis: a fixed joint and a prismatic joint are placed between the base of the model and ground. Thus, with the joints between the base element and ground, the deployable mechanism can be assumed to be in a static state. The final analysis model of deployable mechanism created in ANSYS is shown in Fig. 25.

The coordinate system is defined with horizontal X, Y axes and the vertical Z-axis, the X-axis directed from the fixed joint O to the prismatic joint located at point P_2, the vertical Z-axis points from unit 1 to unit 3.

7.2. Static compression stiffness

As the mechanism has one degree of freedom, locking the actuating joint can guarantee that the whole mechanism has been fixed. However, increasing the number of locked joints is obviously expected to increase the stiffness of the mechanism. In this section, the static analysis is performed under four different combinations of locked joints on the base mast unit: (a) only the actuated joint O' of the base module (the central joint in Fig. 22); (b) the central joints on two adjacent faces of the base unit; (c) the central joints on two opposite faces; and (d) locking all four central joints.

The loading force F_P is along the deployment axis in a top-down direction, and is uniformly distributed at the four vertices of the mechanism. The magnitude of the force at each vertex is 50 N in the model. Fig. 25 shows the loading forces of the model, while Fig. 26 gives the analysis results in each case.

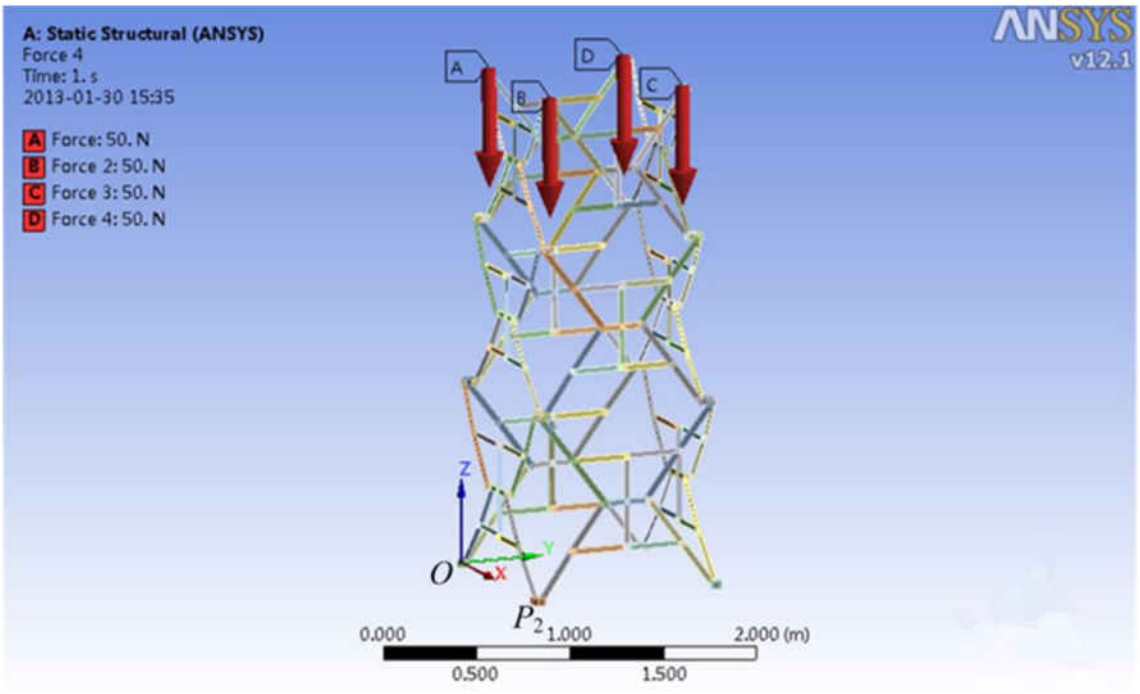

Fig. 25. Analysis model in ANSYS and the applied force for the compression stiffness analysis.

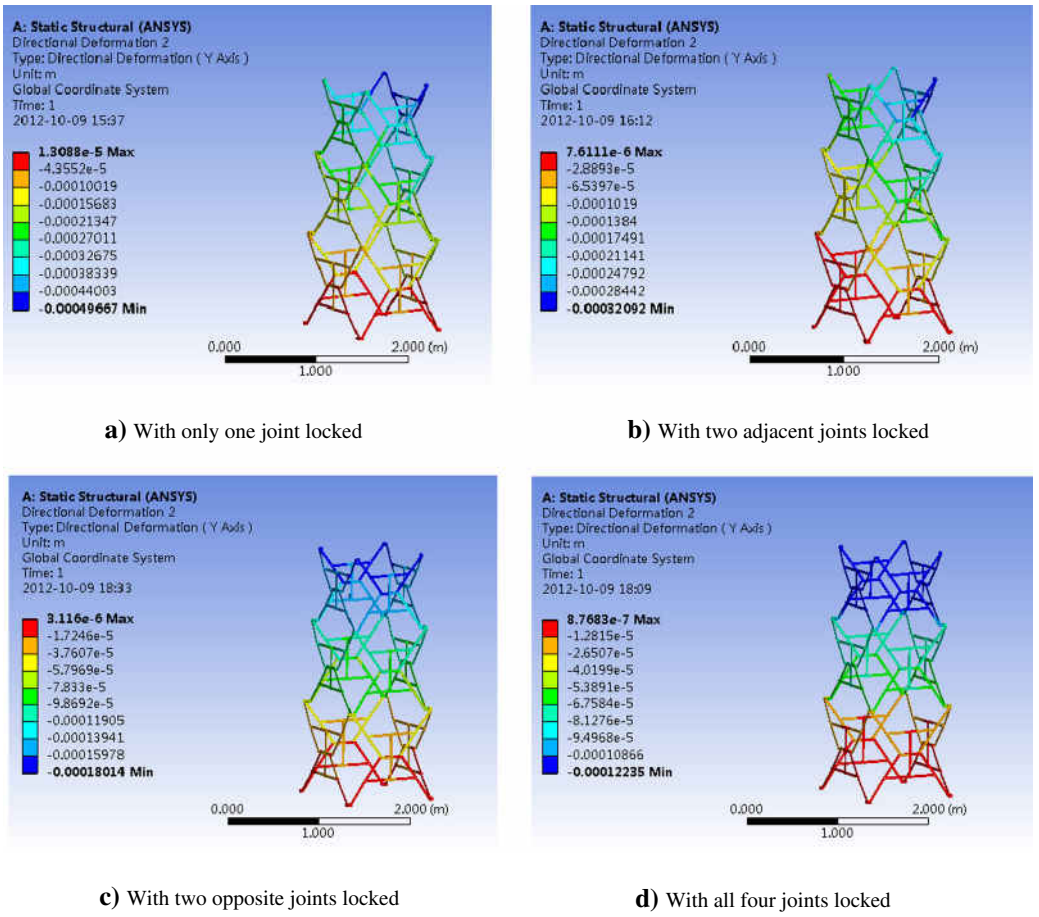

a) With only one joint locked

b) With two adjacent joints locked

c) With two opposite joints locked

d) With all four joints locked

Fig. 26. Maximum deformation of the vertex point under different conditions.

The maximum deformation with forces applied at the vertex is shown in Fig. 26(a). The maximum deformation is 0.497 mm in the first condition, which occurs at the top of the mechanism, where the force is applied.

The relationship between the deformation and static stiffness of the structure is

$$k_c = \frac{F_P}{\delta} \tag{51}$$

where k_c is the compression stiffness, δ is the displacement of the end effector and *Fp* is the loading force.

The compression stiffness of the four locked structures is shown in Table 1.

The fourth condition has the best stiffness, followed by the third condition, while the lowest stiffness is in the first condition. If only one joint is locked, the top surface formed by the four vertexes is inclined, which is undesirable.

7.3. Static bending stiffness

The boundary condition of the bending stiffness is defined as that of the compression stiffness analysis. Several loading forces perpendicular to the deployable axis and a profile of the deployable mast have been distributed on the surface, as shown in Fig. 27. The magnitude of each force is $F_i = 5$ N.

Table 1
Compression stiffness under different conditions.

Locking condition	Compression stiffness (N/m)
One central joint	4.03×10^5
Two adjacent central joints	6.23×10^5
Two opposite central joints	1.11×10^6
All four central joints	1.63×10^6

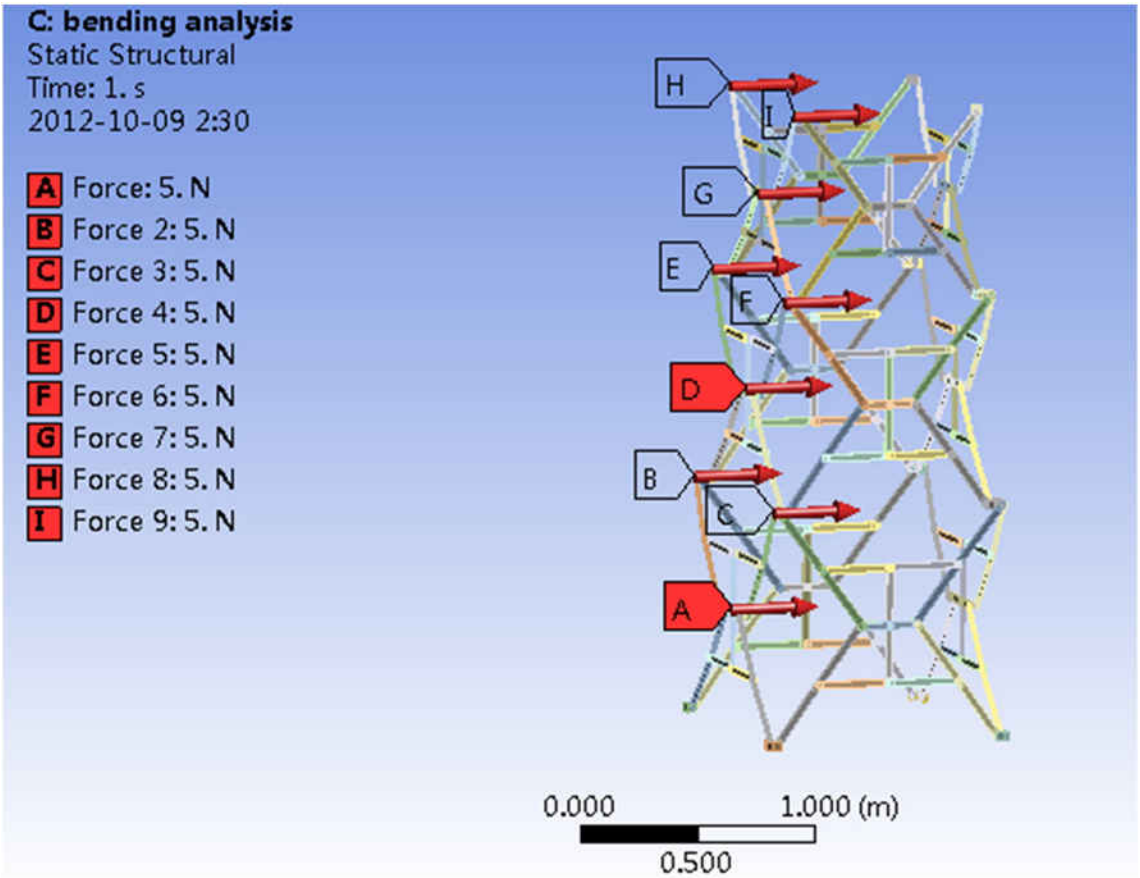

Fig. 27. Applied forces used in the bending stiffness analysis.

The moment applied on the mechanism is:

$$M_F = \sum_{i=1}^{9} F_i L_i = F_i \sum_{i=1}^{9} L_i \tag{52}$$

where L_i is the distance from the i-th force to the base.

We assume that the bending force is perpendicular to the profile. Therefore, we need to differentiate between three different bending scenarios: with one locked joint, two adjacent, two opposing, and four locked joints, Fig. 28. The red circle denotes the locked joint, and the black arrow indicates the direction of the bending force.

For link lengths $l_1 = 0.2$ m, $l_2 = 0.1$ m, $l_3 = 0.25$ m, and $l_4 = 0.25$ m, the total moment applied on the mechanism is $M_F = 78.9375$ Nm. The maximum deformations under each condition are shown in Figs. 29–32. From the deformation results, the maximum bending deformation is 0.18 mm, which occurs at the top vertex of the mechanism with the first locking condition.

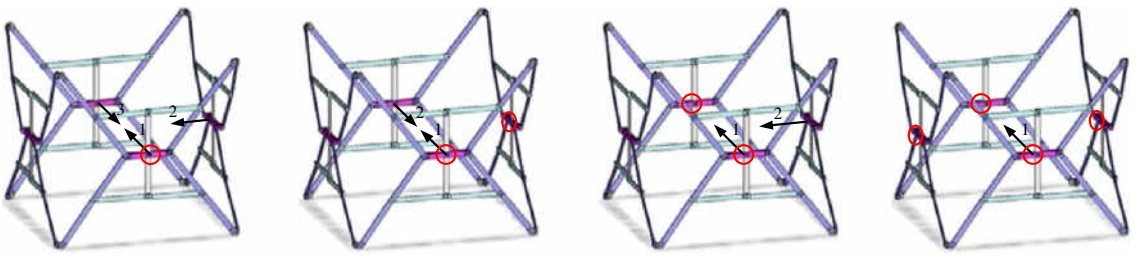

Fig. 28. Bending forces under different locking conditions. (For interpretation of the references to color in this figure, the reader is referred to the web version of this article.)

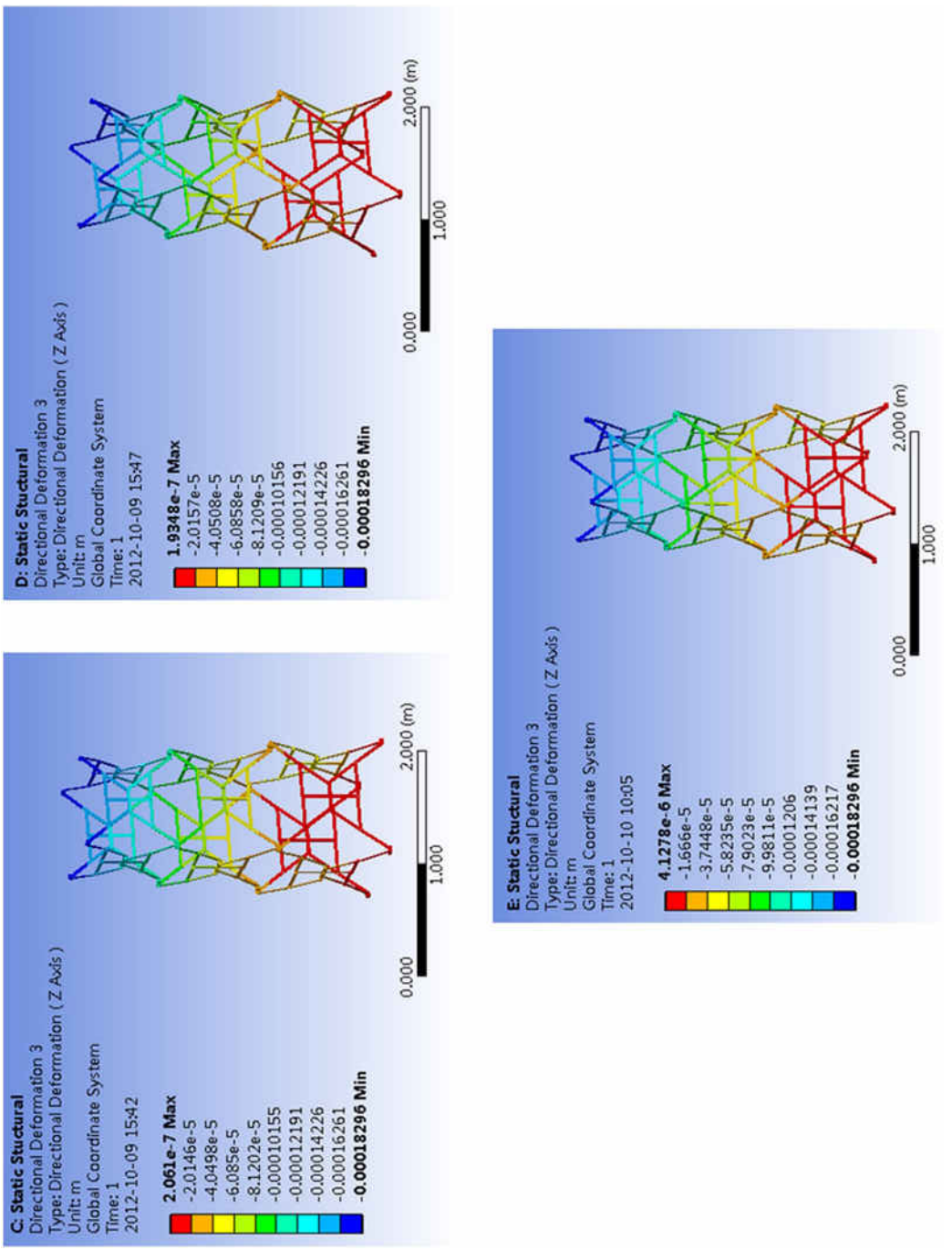

Fig. 29. Maximum deformation with only one joint locked.

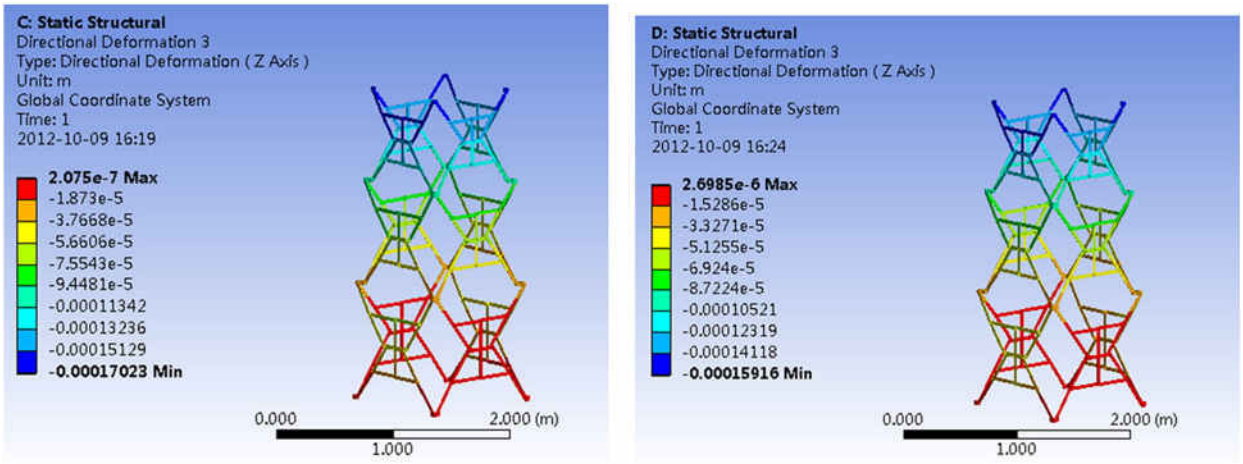

Fig. 30. Maximum deformation with two adjacent joints locked.

The relationship between the deformation and bending stiffness of the structure is

$$EI = \frac{M_F}{\rho} \tag{53}$$

where M_F is the moment applied on the mechanism, and ρ is the deflection of the top vertex of the third unit.

The analyzed bending stiffness of the four conditions is shown in Table 2.

By comparing the results, it can be concluded that the fourth condition also has the best bending stiffness, followed by the third one, while the condition of only one joint locked has the lowest stiffness. However, the influence of the number of locking joints on the bending stiffness is not as pronounced as on the compression stiffness.

7.4. Natural frequency

The relationship between the number and position of the locking joints and the natural frequency of the deployable mast can be observed by using the above model. The natural frequency of the mechanism is analyzed in ANSYS, and the results are shown in Table 3.

Again, the condition with four joints locked has the best performance, but the difference is small. Even with only one joint locked, the mechanism can meet the common requirements of relevant engineering applications.

Based on the above analysis, the following conclusions can be drawn:

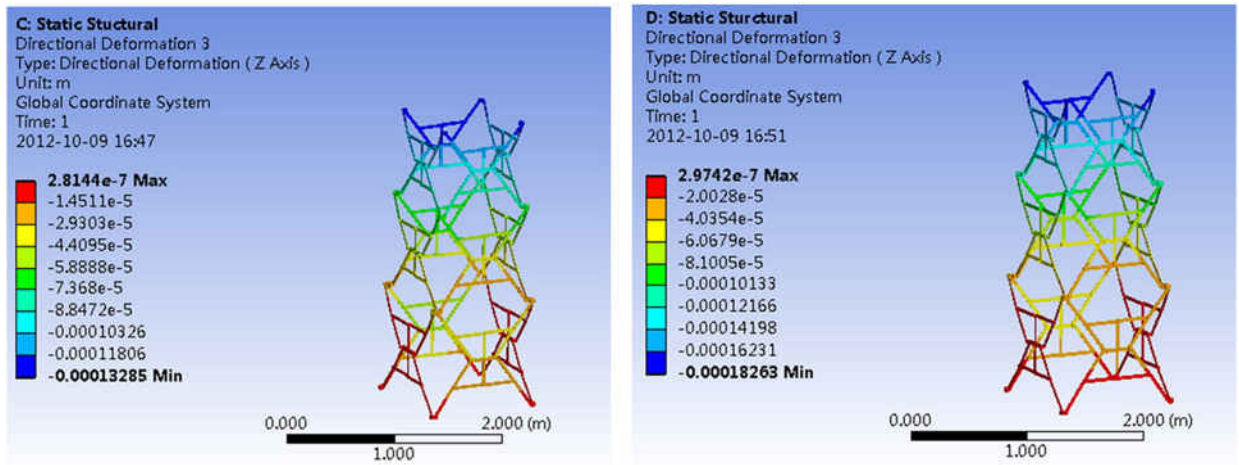

Fig. 31. Maximum deformation with two opposite joints locked.

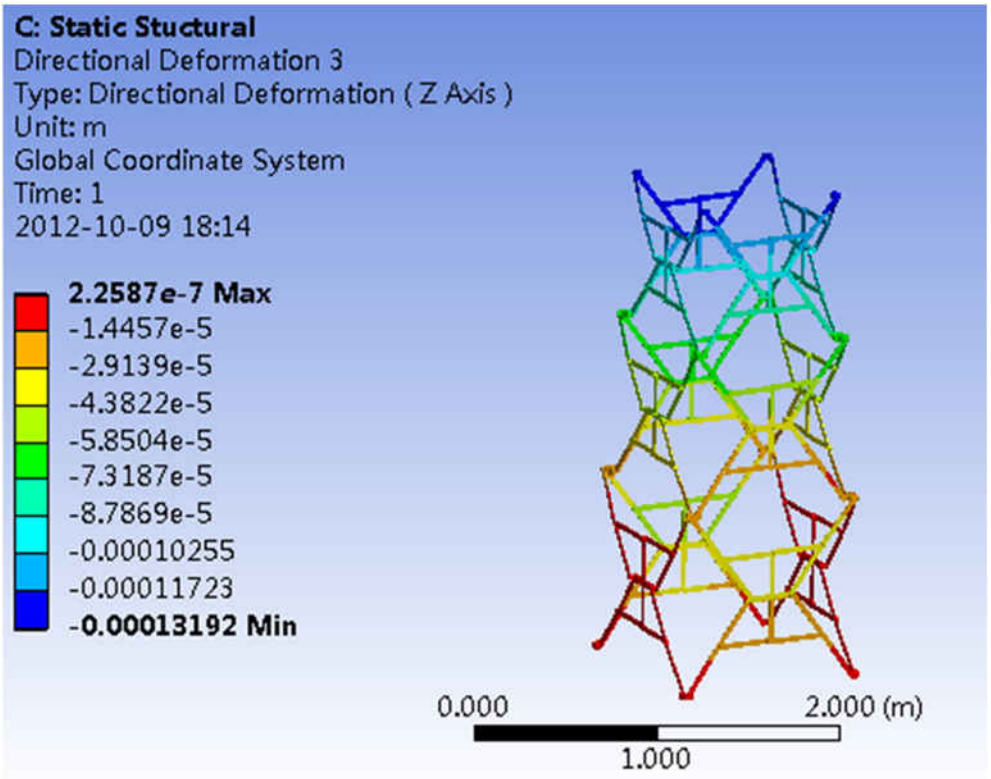

Fig. 32. Maximum deformation with all four central joints locked.

1. Increasing the number of locked joints will improve the structural behavior of the mechanism; it has a significant influence on the compression stiffness, and a smaller one on the bending stiffness and the natural frequency.
2. The end cross section will incline if the locking is not symmetric.
3. In common engineering applications, the compression stiffness of a space-deployable mast should be at least 9×10^5 N/m, the bending stiffness not smaller than 1.47×10^4 Nm^2, and the first-order natural frequency more than 1 Hz. The performed analysis shows that the proposed mechanism is able to meet these standards with two opposite or all four central joints locked.
4. By comparing the third and fourth condition, it can be concluded that the locking of two opposing central joints is the most economical method for fixing the proposed mechanism.

Table 2
Bending stiffness under different conditions.

Condition	Bending stiffness (N m^2)		
	1	2	3
Locking one joint	1.05×10^6	1.05×10^6	1.05×10^6
Locking two adjacent joints	1.13×10^6	1.20×10^6	
Locking two opposite joints	1.44×10^6	1.05×10^6	
Locking all the four joints	1.45×10^6		

Table 3
Natural frequency under different conditions.

Locking condition	Natural frequency (Hz)					
	1	2	3	4	5	6
One joint	10.622	11.079	19.132	22.471	27.049	28.564
Two adjacent joints	10.806	11.934	22.346	24.073	27.167	29.022
Two opposite joints	11.064	13.087	22.324	23.187	27.187	29.118
All four joints	13.036	13.17	22.617	26.082	27.685	29.94

5. The mechanism has the ability of repeatability and high packing efficiency, which makes it suitable for use in several practical applications, e.g. in space as a deployable mast, as the base of reconfigurable fixture of metal sheet parts in industry, and as deployable structure for civil engineering applications.

In addition, in practical engineering applications, cables can be used to improve the stiffness of the mechanism. Tension cables will largely augment the stiffness both in bending and in torsion, but will have little impact on the compression stiffness.

8. Conclusion

In this paper, a novel planar deployable mechanism, which uses the Hoekens straight-line linkage as a basic component, is described and analyzed. The PDM has the ability of altering its size in only one dimension, while width in the perpendicular direction is invariable. The range of straight-line motion is obtained through kinematic analysis, a general static analysis of the linkage is performed, and its singularities are identified. The influence of the physical link size on the magnification ratio is calculated. The basic principles of forming a large deployable mechanism to a desired shape are formulated and applied to propose a family of deployable mast units with invariable cross section and one degree of freedom. Deployable mast units are used to assemble a deployable prism. Kinematic simulation results of the prism deployable mechanism verify the validity of the calculated results. The best location of the actuating joint is obtained through static analysis. Structural performance under different locking conditions and loading scenarios is analyzed in ANSYS, confirming that the proposed mechanism can be used in engineering applications, and several usage recommendations are given.

The theoretical results obtained in this paper have a general validity for deployable mechanisms. As long as the combining conditions are satisfied, the investigated PDM can be used as a unit mechanism in other ways, for instance to form a tiling of the plane.

Acknowledgments

This research has been supported by the National Natural Science Funds (of China) for Distinguished Young Scholar under Grant 51125020, the National Natural Science Foundation of China under Grant 51275015, and the AUTORECON project funded under the Seventh Framework Program of the European Commission (Collaborative Project NMP-FOF-2011-285189).

References

[1] S. Pelegrino, S.D. Guest, Deployable structures: theory and applications, Proceeding of the IUTAM-IASS Symposium, Cambridge, Kluwer Academic Publishers, Dordrecht, 2000, (September 6–9).
[2] C.J. Gantes, E. Konitopoulou, Geometric design of arbitrarily curved bi-stable deployable arches with discrete joint size, Int. J. Solids Struct. 41 (2004) 5517–5540.
[3] C.M. Gosselin, D. Gagnon-Lachance, Expandable polyhedral mechanisms based on polygonal one-degree-of-freedom faces, Proc. Inst. Mech. Eng. C J. Mech. Eng. Sci. 220 (2006) 1011–1018.
[4] J.S. Zhao, F.L. Chu, Z.J. Feng, The mechanism theory and application of deployable structures based on SLE, Mech. Mach. Theory 44 (2009) 324–335.
[5] G.W. Wei, X.L. Ding, J.S. Dai, Mobility and geometric analysis of the Hoberman switch-picth ball and its variant, ASME J. Mech. Robot. 2 (3) (2010) 031010-1–031010-9.
[6] K. Wohlhart, Regular polyhedral linkages, Proceeding of the Second Workshop on Computational Kinematics, Seoul, 2001, pp. 239–248.
[7] C. Hoberman, Radial expansion/retraction truss structures, US Patent 5024031, 1991.
[8] G. Kipper, E. Soylemez, A.U. Ozgur, A family of deployable polygons and polyhedral, Mech. Mach. Theory 43 (2008) 627–640.
[9] W.J. Chen, Y.Z. Luo, G.Y. Fu, et al., A study on space masts based on octahedral truss family, Int. J. Space Struct. 16 (1) (2001) 75–82.
[10] B.P. Nagaraj, R. Pandiyan, A. Ghosal, Kinematics of pantograph masts, Mech. Mach. Theory 44 (2009) 822–834.
[11] X.L. Ding, Y. Yang, J.S. Dai, Topology and kinematic analysis of color-changing ball, Mech. Mach. Theory 46 (2011) 67–81.
[12] R.L. Norton, Design of Machinery, Second ed. McGraw-Hill, New Delhi, 1999.
[13] R.M. Murray, Z.X. Li, S.S. Sastry, A Mathematical Introduction to Robotic Manipulation, CRC Press, 1994.
[14] J.M. Selig, Geometric Fundamentals of Robotics, Springer, 2005.
[15] D. Zlatanov, R.G. Fenton, B. Benhabib, A unifying framework for classification and interpretation of mechanism singularities, Trans. ASME J. Mech. Des. 117 (4) (1995) 566–572.